Revision 1:

Experimental temperature cycling as a powerful tool to enlarge meltpools and crystals at magma storage conditions

MARTIN ERDMANN[1] AND JÜRGEN KOEPKE[2]

[1,2]Institut für Mineralogie, Leibniz Universität Hannover, Callinstr. 3, 30167 Hannover, Germany;

[1]CRPG, UMR 7358, CNRS, Université de Lorraine, 15 rue Notre Dame des Pauvres, 54501 Vandoeuvre-lès-Nancy, France;

E-mail: [1]m.erdmann@mineralogie.uni-hannover.de; [2]koepke@ mineralogie.uni-hannover.de

Phone: [1]+49 (0)511 762 5074; [2]+49 (0)511 762 4084

ABSTRACT

Experiments in high silica systems at temperatures close to the solidus often produce crystals and melt pools which are too small for *in-situ* analysis. Oscillating the temperature during an experimental run speeds up recrystallization of magma by dissolving small and increasing the size of larger crystals, dramatically changing the crystal size distribution. This principle of periodic heating and cooling, caused for example by repeated injection of hot magma, is also a potential acceleration for the formation of phenocrystic textures in natural rocks.

Here we show that temperature cycling has the potential to significantly enlarge melt pools and crystals in a fluid saturated dacitic system. Using a natural dacite dredged from the Pacific-Antarctic Rise as starting material, we performed crystallization experiments applying temperature cycling systematically for two different temperatures and different water activities at 200 MPa. For experiments at 950°C (with $a H_2O$~1, ~0.3, and <0.1) an internally heated pressure

vessel was used, experiments at 800°C (with aH_2O~1, ~0.5) were performed in a cold seal pressure vessel. Comparative experiments at equilibrium conditions with constant temperature were performed for both approaches. For all other experiments temperature was cycled with amplitudes of 20K for different time intervals but constant total run duration after initial equilibration at constant temperature. Additionally, for one experiment at 800°C, the temperature was increased several times by 50 K to study the potential of dissolving tiny crystals in the matrix.

As a result of the temperature cycling, tiny crystals in the matrix were preferentially dissolved, leading to large melt pools with only rare mineral inclusions enabling microprobe analysis using a defocused beam. With regard to the area of the 10 largest crystals of each cycling experiment, clinopyroxene crystals were up to 19 times larger, and plagioclase crystals even up to 69 times when comparing to experiments performed at constant temperature. Grain sizes of FeTi-oxide phases are less influenced by this technique. Essential requirements for applying temperature cycling routinely are identical phase relations and compositions in runs with constant and cycled temperature. For all studied temperatures and water activities, the phase assemblage was the same and compositions of all phases are identical within the analytical error. Thus, the temperature cycling technique opens interesting perspectives, especially in facilitating *in-situ* analysis in near solidus systems.

Keywords: Experimental petrology, Temperature cycling, Crystallization experiments, Dacite, Crystal growth, Phenocrysts

INTRODUCTION

In-situ analyses of experiments by thermal emission techniques in high-silica systems, especially at conditions close to the solidus, are challenging due to the generally very small size of crystals

and melt pools. It is difficult to measure and identify phases with sizes around 1 µm by electron microprobe, and analyses of melt pools < 5 µm by electron microprobe are challenging, due to the requirement of a defocused beam in order to avoid Na-loss (e.g., Morgan and London 2005). Moreover, trace element analyses of experimental phases < 20µm, for example with secondary ion mass spectroscopy (SIMS) or laser ablation ICP-MS, are virtually impossible for these samples. While the positive effect of oscillating temperature on nucleation and growth rates has been well known for decades from material (e.g., Randolph et al. 1971) and food sciences (e.g., Donhowe and Hartel 1996), Mills et al. (2011) showed that for magma analogues it is possible to generate larger phases in experimental run products under atmospheric conditions and at low temperature (47±3°C) via a process of dissolution/recrystallization. In addition, Mills and Glazner (2013) presented a detailed experimental study on the effects of temperature cycling on coarsening of crystals (plagioclase and olivine) in an alkali basalt at ambient pressure.

Previous experimental and petrological studies concentrated less on temperature cycling but rather on effects of decompression and/or cooling rates on crystal size distribution (CSD) in order to understand the formation of phenocrystic textures (e.g., Kirkpatrick 1977; Pupier at al. 2008; Brugger and Hammer 2010). As all of them mainly investigated crystal growth rates and crystal orientation, potential effects on phase chemistry caused by varying temperature remain unconsidered. Moreover, up to now, temperature cycling was rarely studied under pressurized fluid saturated magma storage conditions (Mills and Glazner 2011a).

Here we show that temperature cycling also substantially increases the grain size of the phases (mainly plagioclase, clinopyroxene and melt pools) in a fluid-saturated dacitic system under pressure with varying water activities at magma storage conditions. Particular attention was paid to potential variations of phase chemistry in experiments with temperature cycling compared to

static ones. Some experiments were performed in a cold-seal pressure vessel (CSPV) in which run durations of up to 4 weeks are generally required to generate measureable crystals. This long time duration often causes nickel (the main constituent of the vessel) contamination of the sample due to in-diffusion of Ni through the Au-capsule (Schier and Schmidbaur 1996). Additionally, if the temperature is relatively high (i.e., > 700°C), long run durations causes the vessel to deform. Thus, a further aim of this study was to test the option of reducing the total run duration by applying the temperature cycling technique in this device.

THE APPARATUS

The experiments at 950±20°C were performed in a vertically mounted internally heated pressure vessel (IHPV) using pure argon as pressure medium in the high pressure lab of Hannover, equipped with a rapid quench system to prevent the formation of metastable quench phases (Berndt et al. 2002). The temperature during the experiments was programmed and monitored with a Eurotherm 906 EPC controller. Near-solidus experiments (i.e., T = 800±20°C and +50°C, respectively) were performed in a CSPV with H_2O as pressure medium and external cooling via compressed air. Temperature cycling in the CSPV was programmed by a RKC instrument program controller REX-P24.

The water activity (aH_2O) of the experimental run products was calculated following the thermodynamic model of Burnham (1979, 1994). It should be noted that the model of Burnham (1979) slightly overestimates water activity (e.g., Botcharnikov et al. 2005).The experiments were performed with known hydrogen fugacity (fH_2) corresponding to the intrinsic conditions of the vessels but variable water fugacity (fH_2O). Therefore, the oxygen fugacity (fO_2) is not strictly constant from one capsule to the other. Decreasing fH_2O (accompanied with decreasing initial H_2O in the capsule) causes a lowering of fO_2 (Scaillet et al. 1995). Knowing fH_2O (calculated

after Pitzer and Sterner (1994) from thermodynamically conditions at certain temperature) and fH_2, fO_2 can be computed. Here fH_2 is calculated by the set ΔQFM value for water-saturated conditions of the vessel (QFM = the quartz-fayalite-magnetite buffer; intrinsic conditions of the IHPV (measured with Ni-Pd solid sensors; Taylor et al. 1992): 3.2 log units above fO_2 of QFM, hereafter labeled ΔQFM+3.2; intrinsic condition of the CSPV: ΔQFM+1 corresponding to the Ni-NiO buffer). With given pressure, temperature, and intrinsic pH_2 conditions, ΔQFM for water saturated conditions was calculated following models of Pitzer and Sterner (1994), Shaw and Wones (1964), and Schwab and Küstner (1981). Considering the variation of aH_2O in our runs, the estimated values of fO_2 of our experiments vary between ΔQFM-0.4 and ΔQFM+3.2 (Tab. 1). With regard to natural systems, this is generally more oxidizing than in typical MORB magmas (Bézos and Humler 2005). However, since we expect a higher aH_2O prevailing during the corresponding late-stage magmatic processes, and since water has an oxidizing effect (e.g., Botcharnikov et al. 2005), we expect generally a higher fO_2 for the formation of silicic melts compared to primary MORB processes.

The chosen pressure for the experiments was 200 MPa, which is a typical value for magma storage conditions at the base of fast-spreading oceanic crust. Moreover, at this pressure several phase equilibria studies have been performed for more primitive tholeiitic systems, which make our results directly comparable to experimental data of those studies (e.g., Berndt et al. 2005; Botcharnikov et al. 2008; Feig et al. 2006, 2010).

THE STARTING MATERIAL

As starting material for the temperature cycling study, we used a remelted natural glass from the Pacific-Antarctic Rise (PAR) with dacitic composition (Tab. 2; sample 3DS1 from Haase et al. 2005). The study presented here was performed in the framework of a phase relation study which

aims to experimentally simulate the generation of felsic melts in oceanic crust. The natural sample is analytically well characterized (major and trace elements, selected isotopes) and can be regarded as an evolved end-member in the magmatic evolution of the PAR from MORB to felsic melts. The mineral assemblage in this sample consist of small (~0.2 mm) plagioclase and clinopyroxene phenocrysts in a glassy matrix with accessory oxides (< 10 μm). Detailed petrographical and geochemical information for sample 3DS1 and other characteristic evolved lavas are presented by Freund et al. (2013). Phase equilibria in this system were estimated in a companion study (preliminary results in Erdmann et al. 2012).

For the preparation of the starting glass we followed Feig et al. (2006). The sample was crushed and ground in a rotary mortar. The powder was fused twice at 1600°C in a platinum crucible at 1 atm (so at highly oxidizing conditions, where Fe diffusion into the capsule material is negligible) and quenched by placing the crucible in water. Between the two fusing steps, the glass was ground again. The homogeneity of the glass was checked by electron microprobe on pieces from the top, middle, and bottom of the crucible. Fe and Na loss of the fused glass compared to the whole rock analysis of the natural starting material (water free sample PAR-SO157-3DS1 of Freund et al. 2013 normalized to 100 wt%) is minimal (FeO 7.87 wt%/8.15 wt%, 4.45 wt%/4.59 wt%). The starting material for the experimental runs was produced by grinding the glass in two different fractions (<125 μm and 125-200 μm). These two fractions were mixed together in a ratio ~1:1 to reduce the free volume between grains.

Au-capsules were used for the experiments with 40 mg starting glass powder and a defined amount of fluid. For studying the influence of water, aH_2O of the experiments was fixed via a mixture of deionized water and CO_2 (by using silver-oxalate, $Ag_2C_2O_4$). At one run (defined P, T,

fH_2), several experiments can be performed simultaneously. All were fluid-saturated (~5 % total fluid) with different H_2O-CO_2 proportions, verified by bubbles observed in each experiment.

EXPERIMENTAL PROCEDURE TO ENLARGE MELT-POOLS AND CRYSTALS

Several static reference experiments (identical run conditions with respect to duration, mean temperature, redox conditions, and water content) were performed to monitor the influence of temperature cycling on phase appearance and composition. For this, static experiments were compared with runs of different length of thermal cycling intervals. Additionally, experiments above and below the temperatures chosen for cycling (i.e., 950°C and 800°C, respectively) were performed in order to consider all potentially crystallizing phases (preliminary results presented by Erdmann et al. 2012). This is crucial as phase relations have to be known and potential transgression of phase stability fields due to varying temperature has to be taken into account. To illustrate this, a simplified phase diagram for high aH_2O is presented in Figure 1 where phase-in boundaries are potentially overstepped.

Two cycling experiments at 950°C using an IHPV were initially equilibrated at constant temperature for 40 h in order to generate first crystals at identical conditions as in static runs. Afterwards, the first run was cycled three times for 13 h with 11 h of constant temperature in between (72 h in total). The second run was cycled for 72 h without interruption. The two different approaches (i.e., alternate cycling and static run and solely cycling) were chosen to test of whether equilibration at constant temperature is necessary to generate the same phase composition as in entire static runs. In both cases the experiments were finally equilibrated for 8 h, so that the total run time was always 120 h. Amplitudes (α) were 20 K (maximum possible value without overstepping phase boundaries except for amphibole; see simplified phase diagram in Fig. 1) with periods (τ) of 40 min (including heating up and cooling down time with a ramp of

20 K/min; 40 min is the shortest possible time without running the risk of an uncontrolled oscillating of the furnace). The overshoot caused by rapid heating/cooling was 5 K and the temperature was stable (±0.5 K) after ~3 min (Fig. 2).

Applying the temperature cycling technique in CSPV's is more challenging in terms of controlling the sample temperature and keeping the pressure constant as the vessel is externally heated. As typical for CSPV's, cooling and heating proceeds more slowly than in IHPV's. Thus, chosen τ was longer than in IHPV experiments (120 min instead of 40 min) with the same α (i.e., 20K). Heating and cooling rates are not constant but fast at the beginning and decelerated close to the target temperature with the result that overshooting was not observed (Fig. 2). The target temperature (±1°C) was reached after 30 min. Total run duration was 336 h/14 days with 192 h/8 days of cycling, 96 h/4 days initial and 48 h/2 days final equilibration. In addition to the temperature cycling runs, a peak temperature series was performed with the idea to keep the temperature constant for most time, omit the kinetically ineffective time at lower temperatures, and quickly dissolve tiny crystals at distinctively higher temperature. For this, temperature was maintained at 800°C for most time with short (1 h) increases up to 850°C. In order to guarantee comparable conditions to temperature cycling experiments, initial (96 h) and final (48 h) equilibration were adopted from cycling experiments. In between, temperature was increased for 1 h up to 850°C, and then held for 5 h at 800°C. This was repeated 32 times. Heating up to 850°C (±2°C) and cooling down to 800 °C (±2°C) proceeded within 24 min (cf. T distribution in Fig. 2).

As the bomb of the CSPV is closed during the experiment, internal pressure is influenced by heating and cooling. However, pressure during the experiment was constant at 200 MPa (±5) at 800°C when no temperature cycling was operating. While heating up to 820°C pressure increases to maximal 219 MPa and decreases to 184 MPa at 780°C. Heating up to 850°C causes a pressure

increase up to 245 MPa. However, this relatively high pressure prevailed for less than 10 % of total run duration (32 of 336 h) as main temperature was 800°C where pressure was constant at 200 MPa (±5). Moreover, pressure change of less than 20 MPa for temperature cycling and even of 45 MPa at the peak temperature series are considered to be negligible (e.g., Feig et al. 2006). This is confirmed by the static comparative test with the same total duration in which pressure was constant and water content at water saturated conditions was the same as in cycling experiments. It is well known that water content is pressure dependent (e.g., Feig et al. 2006). Thus, if the average pressures in the cycling experiments would have been different, the water concentrations in the melt would have been different, which was not observed.

Additionally, static experiments for 650 h/27 days for the different water activities were performed, as this is considered to be required for equilibrium conditions in high-silica systems (74 to 79 wt% SiO_2 in melt; cf. Tab. 2).

ANALYTICAL METHODS

The run products (glass and minerals) were analyzed with the Cameca SX 100 electron microprobe at Leibniz Universität Hannover, Germany. For the analyses of the crystals, following operating conditions were chosen: 15 kV high voltage, 15 nA beam current, 10 seconds counting time on peak and 10 s on background, focused beam. For the analyses of the remaining melt (water-bearing), which is problematic due to "alkali-loss" effects (e.g., Morgan and London 2005), a special procedure was applied following Koepke et al. (2004). The beam current was set to 4 nA, the counting time varied for the corresponding elements and was 4 s for K, 8 s for Si, Al, Ti and Fe, 10 s for Na and Zr, 12 s for Mg, 16 s for Ca and 30 s for P, Cl and Mn. Na and K were counted first on their spectrometers. Background counting time was always same as the peak time. Whenever possible, a defocused beam with a spot size of 5, 10 or 20 µm was used, and Na-

loss was checked by comparing the results of measurements with different beam size on identical glasses of an experimental sample with larger melt pools. Standard glasses with composition similar like the experimental glasses and with known water content (analyses of melt and standard glasses with according water content calculation via by-difference are listed in the deposit material) have been used for estimating the water contents in the experimental glasses by the "by-difference" method (Devine et al. 1995).

RESULTS AND DISCUSSION

Achievement of equilibrium

Run durations as long as possible are the best way to attain near-equilibrium conditions in experiments, especially in highly polymerized melt compositions. In this study a variation of run duration at constant P-T conditions, fO_2 and aH_2O was only performed at one series at 800°C in the CSPV. However, run durations for all other experiments in the IHPV and CSPV are expected to be sufficient since they were conducted in a similar time frame as experiments with rhyolitic starting material in the same IHPV (Almeev et al. 2012) and distinctly longer than experiments on a hydrous tholeiitic basalt (Feig et al. 2010).

The following observations suggest that equilibrium was obtained: (1) Crystals and melt are distributed homogenously along the capsule; (2) crystals are euhedral and chemically constant within one experimental run (i.e., low standard deviation; Tab. 2); (3) melt measurements are also constant within the analytical error; (4) the compositions of crystals and melt change with the experimental conditions, following expected compositional trends; (5) static experiments were reproduced twice in temperature cycling experiments with the same total run duration and consistent melt and crystal chemistry (see below).

Effect of temperature cycling on phase relation

Experiments performed at 950°C in the IHPV. By comparing the static experiment (i.e., constant temperature for the complete run duration) at 950°C with experiments initially equilibrated at the same temperature but cycled ±20 K for different time spans, a significant change in texture can be observed (Fig. 3). While tiny crystals of clinopyroxene and plagioclase residing in the matrix were dissolved, these phases were enlarged significantly in general. This is most effective for clinopyroxene at high $a\mathrm{H_2O}$ (Fig. 3 *I*) where only one large single crystal is present after cycling. This clinopyroxene is 19 times larger in area (1350 µm²) than the largest clinopyroxene in the static run # 42 (70 µm²; Tab. 3). The apparent coarsening of plagioclase due to temperature cycling at 950°C increases with decreasing water activity and shows a maximum effect at $a\mathrm{H_2O}$ <0.1. In run #66 the average measured area of the 10 largest plagioclase crystals (determined via *ImageJ*; Schneider et al. 2012; http://imagej.nih.gov/ij/) is 114 µm² and, thus, 69 times larger as the area of the 10 largest plagioclases of the static run #45 (1.7 µm²; Tab.3). The area of pyroxene crystals in low $a\mathrm{H_2O}$ runs reveal a maximum enlargement of 240 % for continuous cycling (#66 compared to #45). However, for *in-situ* analyses this enlargement is crucial as it shift the crystals in an easily measureable range (from 2.9 to 9.8 µm² in average of the 10 largest crystals). This enlargement also allows to measure orthopyroxene crystals (<0.5 vol%) which were probably also present in the two other experiments but was too small to be identified. Due to dissolution of tiny phases in the matrix and fewer crystals in general, crystal free melt pools in the cycled runs are larger. Different is the behavior of Fe-Ti oxides (magnetite and ilmenite), which are less influenced by temperature cycling than silicate phases. The numbers of tiny crystals of Fe-Ti oxides in the matrix and as inclusions in other phases are reduced but still observable. Coarsening of these phases is insignificant. For this reason, the effect of temperature cycling is less obvious in experiments with high water activity at 950°C, where

magnetite is the dominant phase and plagioclase not present. However, the striking enlargement of clinopyroxene in these runs described above show that temperature cycling enlarges at least clinopyroxenes most effective at high water activity.

Experiments performed at 800°C in the CSPV. The aim of temperature cycling applied in experiments performed in CSPV's was to shorten the total run duration and enlarge crystals and melt pools simultaneously. Static experiments of 27 days at 800°C and aH_2O~1 (#81) exhibit only slightly larger crystals than the static one with a duration of 14 days (#105). Although experiment #81 bears large crystals (mainly clinopyroxene and amphibole), they are all concentrated at the rim close to the capsule wall, obviously influenced by diffused water, indicated by contamination with Ni up to 10 wt%. Experiment #105 does not show any Ni-contamination after 14 days. However, all phases are relatively small (Fig. 3). The corresponding cycling experiment with α=20 K and a duration of 14 days bear clinopyroxenes with a comparable size (with regard to the area of the 10 largest crystals; see Tab. 3). Plagioclases are 3 times larger in area (62 µm² compared to 20 µm²). Even larger crystals were produced in the peak temperature experiment (T-increase of 50 K every 6 h for 1 h) where plagioclases are 14 times and clinopyroxenes (without Ni contamination) 7 times larger than in the static one (Fig. 3). At reduced water activity the cycling effect is less pronounced but still apparent. The experiment with α=20 K (#103) and especially the one with peak T (#111) show larger crystals than the static reference experiment; however, more obvious are the distinctively larger melt pools, especially in the peak T run #111 (Fig. 3). Cycling run #103 bears, in contrast to static run #107, small amounts of zircon. Similar to the orthopyroxene occurrence in #66 of the IHPV experiment, we assume that zircon was present in the two other experiments (#107 and #111), but was too small to be identified. In all other experiments, phase relations in temperature cycling experiments are

the same as in static ones. In summary, an overstepped phase-in boundary during oscillation is uncritical as long as initial and final equilibration was established.

With regard to phase proportions, a generally good accordance between static and cycling experiments is given. Based on analyzes using *ImageJ* (Schneider et al. 2012; http://imagej.nih.gov/ij/), modal proportions are practically identical (Tab. 1). The strongest variations are observed for cycling run #66 with 7 vol% more melt and peak temperature run #110 with 12 vol% less melt than in the corresponding static ones. This is probably caused by considering sample areas with large crystals and meltpools, respectively, for BSE images. Thus, crystals and meltpools are potentially irregularly distributed on the images analyzed and do not represent the sample average.

Effect of temperature cycling on phase chemistry

Variations of clinopyroxene and plagioclase composition. Phase chemistry of all major phases is given in Table 2. As stated above, clinopyroxenes and plagioclases are mainly influenced by temperature cycling. Thus, the compositions of these two phases are illustrated in Figure 4 for potential variations of all measured elements (given as oxides and normalized to the composition of clinopyroxene and plagioclase of the corresponding static run). Discrepancies between static and cycling experiments are generally small. This implies that equilibration of the phases occur at the very beginning of an experiment and cycling only minor affects the final composition. In general, no chemical zonation was observed despite enormous growth of the crystals. Variations are accentuated when the content of an oxide is small in the phase (e.g., K_2O in clinopyroxene and MgO in plagioclase). Clinopyroxenes of run #57 show additionally lower values for TiO_2 and Al_2O_3 (Fig. 4 *I*) while they are enriched in Na_2O in run #66 (Fig. 4 *III*). The static run at 950°C with $aH_2O<0.1$ (#45) has many tiny phases making analyses of plagioclase

and melt, which are concentrated in the matrix, difficult. Thus, the measurements of these phases (Tab. 2) show probably contaminated values and are omitted in Figure 4 *III* and Figure 5. Variations in phase chemistry of CSPV experiments are also minor and only objectionable for oxides of plagioclase with low contents (i.e., TiO_2 and MgO). Clinopyroxenes of run #103 also show pronounced variations (Fig. 4 *V*). However, the overall good agreement of static and cycling phase chemistry shows that the cycling technique is a valuable tool for increasing the grain sizes of the experimental products without influencing the mineral compositions.

Although Fe-Ti oxides are only marginally enlarged by thermal cycling, they show significant variations in TiO_2 and FeO_{total} contents in some runs (Tab. 2). The most pronounced discrepancy is observed for cycling run #101 with distinctively higher TiO_2 values in magnetite and ilmenite. A possible explanation is the slightly lower melt water content in this run leading to more reducing conditions compared to the reference experiments. This influences Fe-Ti oxide composition but has little effect on other phases.

Variations of melt composition. Melt composition of cycled experiments is normalized to melt composition of the corresponding static runs and illustrated in Figure 5 for all measured elements (given as the corresponding oxide, except Cl). Most distinctive are the variations for P_2O_5 which is mainly due to very low contents in the melt which highlight small variations. Cycling run #62 is additionally slightly enriched in melt MgO compared to the static run and cycling run #57 (Fig. 5 *I*). Experiments performed at low aH_2O (i.e. <0.1) without temperature cycling are lacking in measureable meltpools and are, thus, not illustrated in Figure 5. Cycling runs at these conditions (#65 and #66) show moderate variations, probably caused by slightly different melt water contents (Tab. 2). Runs #101 and #110 are enriched in TiO_2 and vary in the Cl content (Fig. 5 *IV*) while #103 and #111 are distinctively enriched in Na_2O (Fig. 5 *V*),

probably caused by small variations in plagioclase crystallization. However, the general variations of the temperature cycling experiments compared to the static ones are marginal and mostly limited to elements with low contents.

IMPLICATIONS

The aim of this study was to test whether the application of temperature cycling in a dacitic system may help to produce different textures in experiments that allow easier melt analysis with *in-situ* methods. Inspired by the innovative work of Mills et al. (2011), the cycling technique was adopted to the phase equilibria study under pressure and varying water activity, with the goal to obtain larger melt pools and crystals in experiments close to the solidus. As experimental conditions chosen here (i.e., pressure, temperature, redox conditions, water activity) are common for phase relation studies in various magmatic systems, our results have the potential to optimize such experimental approaches and enable experimental petrologists to study their run products for example with *in-situ* trace element techniques as SIMS. We showed that temperature cycling helps to enlarge crystals and melt pools significantly without affecting the phase relations or phase compositions. However, this study only presents first steps for crystal coarsening in a fluid saturated system without considering systematical variations of α and τ in detail, as it was performed by Mills and Glazner (2013) for an alkali basalt at ambient pressure. Since the control of additional parameters like pressure and water-activity which in turn influences the redox conditions is challenging and time consuming, further studies are needed.

Even though experiments are generally designed to simulate natural processes at *equilibrium* conditions (i.e., constant temperature), several processes in nature suggest that oscillating temperature is common. Potential processes responsible for periodic heating and cooling are: (1) Repeated injection of hot magma (Huppert and Sparks 1988); (2) thermal convection (Martin et

al. 1987; (3) variation in water activity. That temperature cycling occurs indeed in nature is inferred for example from K-feldspar megacrysts (Johnson and Glazner 2010; Glazner and Johnson 2013). The experimental confirmation that oscillating temperature causes significant crystal enlargement helps to interpret igneous rock texture, in particular, the generation of phenocrysts. As this is largely governed by the interplay of nucleation and growth rates accompanied with rates of cooling and heating (e.g., Carmichael et al. 1974) the basic conditions are desirable to know. Although we do not consider systematically the effect of τ in this study, we assume that it has less impact on growth rates compared to α indicated by experiment #110 where α (peak) of 50 K enlarges crystals more compared to α of 20 K in #101 at same τ without static time in between. This is supported by Mills and Glazner (2013) who observed little correlation between τ and growth rates in an alkali basalt. Thus, time of temperature change in natural systems seems to be of second order importance, as long as it proceeds in geological short terms (i.e., within days) before a new equilibrium is reached. Then, with increasing temperature, small crystals with a high ratio of surface area to volume are preferentially dissolved relative to large crystals following by reprecipitation onto these large crystals while temperature goes down.

ACKNOWLEDGEMENTS

We thank Otto Dietrich and Julian Feige for their careful sample preparation. We gratefully acknowledge the chief scientists of RV Sonne, especially K.M. Haase, for access to the sample 3DS1 used in this study. Thoughtful and thorough reviews by Allen Glazner, Craig Lundstrom, and Editor Charles Lesher greatly improved the manuscript. Funding for this research was provided by grants from the Deutsche Forschungsgemeinschaft (KO 1723/13). This is CRPG contribution number 2407.

REFERENCES CITED

Almeev, R.R., Nash, B.P., Holtz, F., Erdmann, M., and Cathey, H.E. (2012) High-temperature, low-H2O Silicic Magmas of the Yellowstone Hotspot: an Experimental Study of Rhyolite from the Bruneau-Jarbidge Eruptive Center, Central Snake River Plain, USA. Journal of Petrology, 53(9), 1837-1866.

Berndt, J., Liebske, C., Holtz, F., Freise, M., Nowak, M., Ziegenbein, D., Hurkuck, W., and Koepke, J. (2002) A combined rapid-quench and H2-membrane setup for internally heated pressure vessels: Description and application for water solubility in basaltic melts. American Mineralogist, 87(11-12), 1717-1726.

Berndt, J., Koepke, J., and Holtz, F.O. (2005) An Experimental Investigation of the Influence of Water and Oxygen Fugacity on Differentiation of MORB at 200MPa. Journal of Petrology, 46(1), 135-167.

Bézos, A., and Humler, E. (2005) The Fe3+/[Sigma]Fe ratios of MORB glasses and their implications for mantle melting. Geochimica et Cosmochimica Acta, 69(3), 711-725.

Botcharnikov, R.E., Koepke, J., Holtz, F., McCammon, C., and Wilke, M. (2005) The effect of water activity on the oxidation and structural state of Fe in a ferro-basaltic melt. Geochimica et Cosmochimica Acta, 69(21), 5071-5085.

Botcharnikov, R.E., Almeev, R.R., Koepke, J., and Holtz, F. (2008) Phase Relations and Liquid Lines of Descent in Hydrous Ferrobasalt: Implications for the Skaergaard Intrusion and Columbia River Flood Basalts. Journal of Petrology, 49(9), 1687-1727.

Brugger, C.R., and Hammer, J.E. (2010) Crystal size distribution analysis of plagioclase in experimentally decompressed hydrous rhyodacite magma. Earth and Planetary Science Letters, 300, 246-254.

Brugger, C.R., Johnston, A.D., and Cashman, K. (2003) Phase relations in silicic systems at one-atmosphere pressure. Contributions to Mineralogy and Petrology, 146(3), 356-369.

Burnham, C.W. (1979) The importance of volatile constituents. *In* The Evolution of the Igneous Rocks: Fiftieth Anniversary Perspectives (Yoder, HS, ed.) pp. 439-482. Princeton University Press.

Burnham, C.W. (1994) Development of the Burnham model for prediction of H2O solubility in magmas. *In* Carroll, M. R. & Holloway, J. R. (eds) Volatiles in Magmas. Mineralogical Society of America and Geochemical Society, Reviews in Mineralogy and Geochemistry 30, 123-129.

Carmichael, I.S.E., Turner, F.J., and Verhoogen, J. (1974) Igneous petrology. McGraw-Hill.

Devine, J.D., Gardner, J.E., Brack, H.P., Layne, G.D., and Rutherford, M.J. (1995) Comparison of microanalytical methods for estimating H 2 O contents of silicic volcanic glasses. American Mineralogist, 80(3-4), 319-328.

Donhowe, D.P., and Hartel, R.W. (1996) Recrystallization of ice in ice cream during controlled accelerated storage. International Dairy Journal, 6(11-12), 1191-1208.

Erdmann, M., Koepke, M., Freund, S. (2012) Phase relations and distribution coefficients for evolved lavas from the Pacific-Antarctic Rise. EMPG2012 Conference Abstracts.

Feig, S., Koepke, J., and Snow, J. (2006) Effect of water on tholeiitic basalt phase equilibria: an experimental study under oxidizing conditions. Contributions to Mineralogy and Petrology, 152(5), 611-638.

- (2010) Effect of oxygen fugacity and water on phase equilibria of a hydrous tholeiitic basalt. Contributions to Mineralogy and Petrology, 160(4), 551-568.

Freund, S., Beier, C., Krumm, S., and Haase, K.M. (2013) Oxygen isotope evidence for the formation of andesitic-dacitic magmas from the fast-spreading Pacific-Antarctic Rise by assimilation-fractional crystallisation. Chemical Geology, 347(0), 271-283.

Giordano, D., Russell, J.K., and Dingwell, D.B. (2008) Viscosity of magmatic liquids: A model. Earth and Planetary Science Letters, 271(1-4), 123-134.

Glazner, A. F., and Johnson, B. R. (2013) Late crystallization of K-feldspar and the paradox of megacrystic granites: Contributions to Mineralogy and Petrology, 166, 777-799.

Haase, K.M., Stroncik, N.A., Hekinian, R., and Stoffers, P. (2005) Nb-depleted andesites from the Pacific-Antarctic Rise as analogs for early continental crust. Geology, 33(12), 921-924.

Huppert, H.E., and Sparks, R.S.J. (1988) The Generation of Granitic Magmas by Intrusion of Basalt into Continental Crust. Journal of Petrology, 29(3), 599-624.

Johnson, B. R., and Glazner, A. F. (2010) Formation of K-feldspar megacrysts in granodioritic plutons by thermal cycling and late-stage textural coarsening. Contributions to Mineralogy and Petrology, 159, 599-619.

Kirkpatrick, R.J. (1977) Nucleation and growth of plagioclase, Makaopuhi and Alae lava lakes, Kilauea Volcano, Hawaii. Geological Society of America Bulletin, 88(1), 78-84.

Koepke, J., Feig, S., Snow, J., and Freise, M. (2004) Petrogenesis of oceanic plagiogranites by partial melting of gabbros: an experimental study. Contributions to Mineralogy and Petrology, 146(4), 414-432.

Martin, D., Griffiths, R., and Campbell, I. (1987) Compositional and thermal convection in magma chambers. Contributions to Mineralogy and Petrology, 96(4), 465-475.

Mills, R.D., and Glazner, A.F. (2011a) Experimental evidence for coarsening of crystals and bubbles during thermal cycling of mafic and silicic magmas. Goldschmidt Conference Abstracts: Mineralogical Magazine, 75, 1475.

Mills, R.D., and Glazner, A.F. (2013) Experimental study on the effects of temperature cycling on coarsening of plagioclase and olivine in an alkali basalt. Contributions to Mineralogy and Petrology, 1-15.

Mills, R.D., Ratner, J.J., and Glazner, A.F. (2011) Experimental evidence for crystal coarsening and fabric development during temperature cycling. Geology, 39(12), 1139-1142.

Morgan VI, G.B., and London, D. (2005) Effect of current density on the electron microprobe analysis of alkali aluminosilicate glasses American Mineralogist, 90, 1131-1138.

Pitzer, K.S., and Sterner, S.M. (1994) Equations of state valid continuously from zero to extreme pressures with H2O and CO2. Journal of Chemical Physics, 101(4), 3111-3116.

Pupier, E., Duchene, S., and Toplis, M. (2008) Experimental quantification of plagioclase crystal size distribution during cooling of a basaltic liquid. Contributions to Mineralogy and Petrology, 155(5), 555-570.

Randolph, A.D., Larson, M.A., and Larson, A.D.R.A. (1971) Theory of Particulate Processes. Academic Press, New York.

Scaillet, B., Pichavant, M., and Roux, J. (1995) Experimental Crystallization of Leucogranite Magmas. Journal of Petrology, 36(3), 663-705.

Schier, A., and Schmidbaur, H. (1996) Edelmetall-Taschenbuch, 2., Degussa AG, Frankfurt a.M. Ed. G. Beck, H. H. Beyer, W. Gerhartz, J. Hausselt und U. Zimmer. Hüthig, Heidelberg, 1995. 676 pp., ISBN 3-7785-2448-8. Nachrichten aus Chemie, Technik und Laboratorium, 44(12), 1201-1202.

Schneider, C.A., Rasband, W.S., and Eliceiri, K.W. (2012) NIH Image to ImageJ: 25 years of image analysis. Nature Methods, 9(7), 671-675.

Schwab, R.G., and Küstner, D. (1981) Die Gleichgewichtsfugazitaten technologisch und petrologisch wichtiger Sauerstoffpuffer (The equilibrium fugacities of important oxygen buffers in technology and petrology). Neues Jahrbuch Mineralogische Abhandlung, 140, 111-142.

Shaw, H.R., and Wones, D.R. (1964) Fugacity coefficients for hydrogen gas between O degrees and 1000 degrees C, for pressures to 3000 atm. American Journal of Science, 262(7), 918-929.

Taylor J.R., Wall, V.J., and Pownceby, M.I. (1992) The calibration and application of accurate redox sensors. American Mineralogist, 77, 284–295.

FIGURE CAPTIONS

FIGURE 1. Phase stability fields determined for the composition PAR at 200 MPa and high aH_2O as a function of temperature. On the upper x-axes the approximate water activity is given. Redox conditions are not considered here. Each grey dot corresponds to an experimental run (preliminary results presented by Erdmann et al. 2012). Stars indicate cycling experiments. Dashed lines represent the phase in curves of the corresponding minerals; magnetite (labeled MAG) is the liquidus phase at more oxidizing conditions (mineral abbreviations are the same as in Table 1). The red field indicates the temperature range affected by cycling in IHPV experiments, the green and light green fields the cycling and peak temperature experiments, respectively, performed in the CSPV (experimental data are given in Tab. 2). For interpretation of the references to color in this and the following figures, the reader is referred to the web version of this article.

FIGURE 2. Plot of the experimental temperature profiles investigated in this study. Left graphs show the simplified temperature characteristics in IHPV and CSPV experiments, respectively, with different amplitudes (α) and periods (τ). Small windows on the right show a detailed plot of the logged temperature during cycling including overshoots and delayed heating and cooling. Colors refer to Figures 1, 3, 4 & 5.

FIGURE 3. Comparison of BSE images (with given run number; see Tab. 1 & 2 for run conditions and compositions) of static and cycled runs for different water activities. Roman numbers refer to experimental conditions (Fig. 1) and phase compositions (Fig. 4 & 5). Colors of the experimental run refer to the corresponding temperature profile in Figure 2. Present phases are given in the lower right (abbreviations are the same as in Tab. 1; α = amplitude; τ = period). The analyzed

476 crystals for Table 3 are highlighted in the apart from that same Figure and can be found in the
477 deposit material.

478 **FIGURE 4.** Phase chemistry of clinopyroxene and plagioclase for all measured elements (given as
479 oxides and normalized to the composition of clinopyroxene and plagioclase of the corresponding
480 static run). Roman numbers refer to experimental conditions (Fig. 1) and to BSE images (Fig. 3).
481 Colors of the composition curves refer to the corresponding temperature profile in Figure 2.

482 **FIGURE 5.** Chemistry of experimental melt for all measured elements/oxides normalized to the
483 composition of the corresponding static run. Roman numbers refer to experimental conditions
484 (Fig. 1) and to BSE images (Fig. 3). Colors of the composition curves refer to the corresponding
485 temperature profile in Figure 2.

486

487

488

489

490

491

492

493

494

495

Table 1. Experimental protocol

run	cycling type	P (MPa)	temp. (°C)	time (h)	TC (h)	H_2O[a] by-diff	aH_2O[b] exp	ΔQFM[c] exp	phase assemblages (proportions[d])
#42	static	200	950	120	-	5.1	0.98	+3.2	Melt(95.1), Mag(1.9), Cpx(1.2), Ap(1.8)
#62	TC	200	950±20	120	40	4.9	1.00	+3.2	Melt(96.6), Mag(2.2), Cpx(0.5), Ap(0.7)
#57	TC	200	950±20	120	72	5.1	1.00	+3.2	Melt(95.2), Mag(2.4), Cpx(0.9), Ap(1.5)
#43	static	200	950	120	-	2.6	0.39	+2.2	Melt(63.3), Mag(5.1), Cpx(6.0), Pl(25.6)
#63	TC	200	950±20	120	40	1.8	0.22	+1.9	Melt(66.6), Mag(3.1), Cpx(3.9), Pl(26.5)
#58	TC	200	950±20	120	72	2.0	0.26	+2.0	Melt(67.7), Mag(3.8), Cpx(4.4), Pl(24.1)
#45	static	200	950	120	-	0.5	0.02	-0.3	Melt(24.9), Mag(6.1), Cpx(20.9), Pl(44.1), Qz(4.0)
#65	TC	200	950±20	120	40	0.5	0.02	-0.1	Melt(24.3), Mag(5.7), Cpx(12.9), Pl(53.0), Qz(4.2)
#66	TC	200	950±20	120	72	0.8	0.06	+0.7	Melt(32.0), Mag(3.7), Cpx(15.2), Pl(47.5), Qz(1.6), Opx
#81	static	200	800	650	-	5.5	1.00	+0.6	Melt(72.5), Mag/Ilm(4.9), Cpx(8.2), Pl(14.4), Ap, Zrn
#105	static	200	800	336	-	4.8	0.86	+0.4	Melt(75.9), Mag/Ilm(3.8), Cpx(6.6), Pl(13.7), Ap, Zrn, Amp
#101	TC	200	800±20	336	192	5.5	1.00	+0.5	Melt(68.4), Mag/Ilm(5.7), Cpx(6.7), Pl(19.1), Ap, Zrn, Amp
#110	peak	200	800+50	336	192	5.4	1.00	+0.5	Melt(63.9), Mag/Ilm(3.0), Cpx(13.6), Pl(19.6), Ap, Zrn, Amp
#107	static	200	800	336	-	3.5	0.62	+0.1	Melt(46.7), Mag/Ilm(5.7), Cpx(10.8), Pl(30.9), Qz(6.0), Ap
#103	TC	200	800±20	336	192	2.8	0.43	-0.2	Melt(39.8), Mag/Ilm(6.1), Cpx(8.2), Pl(33.1), Qz(12.9), Ap, Zrn
#111	peak	200	800+50	336	192	3.1	0.50	-0.1	Melt(49.5), Mag/Ilm(6.6), Cpx(9.0), Pl(28.0), Qz(7.0), Ap

Mag magnetite, *Ilm* ilmenite, *Cpx* clinopyroxene, *Opx* orthopyroxene, *Pl* plagioclase, *Qz* quartz, *Ap* apatite, Amp amphibole, Zrn zircon

[a] determination via by-diference (following Devine et al. 1995) with electron microprobe (KFT-calibrated)

[b] water activity is calculated from the measured composition of the fluid phase

[c] ΔQFM indicates log fO_2 (experiment) - log fO_2 (QFM buffer) as estimated by Schwab and Küstner (1981)

[d] phase proportions in vol% (<0.5 vol % if not specified); determined via *ImageJ* (see text for details)

Table 2. Experimental results

Run	Phase	n^a	SiO_2	TiO_2	Al_2O_3	Fe_2O_3	FeO	MnO	MgO	CaO	Na_2O	K_2O	P_2O_5	Cl	ZrO_2	Total
Starting composition		60	65.00 *0.51*	0.95 *0.05*	14.20 *0.21*		7.87 *0.36*	b.d.	1.46 *0.14*	4.58 *0.20*	4.45 *0.26*	1.18 *0.05*	b.d.	0.32 *0.02*	b.d.	100.00
#42	Mag	3	0.08 *0.07*	3.20 *0.04*	1.77 *0.07*	28.48 *0.15*	60.72 *0.45*	0.52 *0.06*	3.04 *0.04*	0.10 *0.01*	b.d.	b.d.				98.01
#62		7	0.13 *0.04*	3.08 *0.05*	1.64 *0.06*	27.97 *0.30*	61.96 *0.44*	0.50 *0.09*	3.51 *0.08*	0.10 *0.05*	b.d.	0.01 *0.02*				98.95
#57		2	0.06 *0.08*	4.28 *0.02*	1.77 *0.01*	29.84 *0.01*	58.22 *0.64*	0.44 *0.00*	2.76 *0.09*	0.07 *0.10*	b.d.	b.d.				97.44
#42	Cpx	5	51.84 *1.09*	0.64 *0.11*	2.89 *0.65*		7.74 *0.65*	0.33 *0.05*	14.01 *0.64*	21.51 *0.86*	0.60 *0.10*	0.09 *0.05*				99.64
#62		3	51.12 *0.24*	0.71 *0.01*	2.25 *0.17*		7.83 *0.10*	0.37 *0.04*	14.82 *0.54*	21.87 *0.41*	0.47 *0.04*	0.04 *0.02*				99.48
#57		2	52.38 *0.27*	0.40 *0.01*	1.28 *0.06*		7.28 *0.04*	0.33 *0.01*	15.48 *0.19*	22.78 *0.33*	0.44 *0.01*	0.02 *0.01*				100.37
#42	Melt	5	67.81 *0.30*	0.89 *0.05*	14.63 *0.12*		4.43 *0.23*	0.15 *0.02*	1.31 *0.07*	4.31 *0.08*	4.61 *0.19*	1.35 *0.06*	0.19 *0.01*	0.32 *0.00*	b.d.	100.00
#62		5	67.26 *0.27*	0.86 *0.08*	14.72 *0.33*		4.41 *0.21*	0.12 *0.01*	1.56 *0.09*	4.62 *0.07*	4.46 *0.19*	1.30 *0.12*	0.23 *0.01*	0.33 *0.00*	0.11 *0.02*	100.00
#57		4	67.52 *0.21*	0.85 *0.05*	14.92 *0.38*		4.37 *0.15*	0.13 *0.03*	1.32 *0.04*	4.34 *0.04*	4.58 *0.22*	1.31 *0.03*	0.21 *0.03*	0.35 *0.00*	0.11 *0.02*	100.00
#43	Mag	4	0.36 *0.18*	7.11 *0.24*	1.91 *0.06*	33.29 *0.58*	51.49 *1.20*	0.55 *0.03*	2.24 *0.11*	0.21 *0.10*	b.d.	0.01 *0.02*				97.18
#63		5	0.52 *0.26*	7.48 *0.07*	1.91 *0.06*	34.30 *0.26*	51.23 *0.28*	0.58 *0.04*	2.11 *0.09*	0.18 *0.06*	0.03 *0.06*	0.02 *0.02*				98.36
#58		3	0.58 *0.60*	8.75 *0.05*	1.93 *0.02*	35.53 *0.45*	47.84 *1.08*	0.51 *0.05*	2.00 *0.12*	0.28 *0.25*	b.d.	0.01 *0.02*				97.44
#43	Cpx	2	51.77 *0.14*	0.75 *0.14*	3.64 *0.71*		9.68 *0.38*	0.51 *0.08*	13.11 *0.71*	19.62 *0.37*	0.93 *0.13*	0.11 *0.08*				100.12
#63		7	51.42 *0.92*	0.70 *0.07*	2.48 *0.52*		10.47 *0.67*	0.54 *0.10*	13.59 *0.35*	19.85 *0.37*	0.74 *0.19*	0.08 *0.05*				99.86
#58		3	51.85 *0.82*	0.53 *0.08*	2.12 *0.32*		10.52 *0.66*	0.54 *0.11*	13.85 *0.56*	19.62 *1.28*	0.64 *0.07*	0.08 *0.07*				99.76
#43	Pl	5	60.11 *0.77*	0.30 *0.08*	21.95 *0.70*		3.23 *0.98*	b.d.	0.72 *0.33*	6.73 *0.30*	6.73 *0.13*	0.38 *0.03*				100.15
#63		5	61.37 *1.09*	0.23 *0.03*	22.63 *0.65*		2.04 *0.37*	b.d.	0.36 *0.18*	6.40 *0.54*	6.70 *0.37*	0.44 *0.10*				100.18
#58		3	59.74 *0.26*	0.19 *0.07*	23.21 *1.19*		2.15 *0.76*	b.d.	0.46 *0.39*	7.05 *0.16*	6.81 *0.37*	0.31 *0.06*				99.92
#43	Melt	3	72.64 *0.59*	0.67 *0.05*	13.04 *0.52*		3.25 *0.12*	0.10 *0.00*	0.58 *0.08*	2.10 *0.30*	5.15 *0.04*	1.73 *0.13*	0.12 *0.02*	0.44 *0.02*	0.17 *0.01*	100.00
#63		3	72.51 *0.47*	0.70 *0.02*	13.37 *0.09*		3.34 *0.22*	0.09 *0.01*	0.52 *0.06*	2.05 *0.01*	4.83 *0.18*	1.83 *0.07*	0.12 *0.00*	0.47 *0.00*	0.15 *0.01*	100.00
#58		3	71.89 *0.92*	0.55 *0.01*	13.59 *0.47*		3.65 *0.21*	0.11 *0.01*	0.55 *0.08*	2.07 *0.25*	5.10 *0.44*	1.82 *0.17*	0.10 *0.01*	0.44 *0.02*	0.13 *0.02*	100.00
#45	Mag	3	0.74 *0.48*	12.03 *0.40*	1.58 *0.11*	40.19 *0.61*	41.39 *1.57*	0.42 *0.05*	1.25 *0.02*	0.25 *0.12*	b.d.	b.d.				97.84
#65		3	1.84 *1.06*	12.62 *0.78*	1.86 *0.43*	40.22 *0.96*	38.70 *1.65*	0.40 *0.05*	0.96 *0.50*	0.59 *0.52*	0.43 *0.40*	0.06 *0.03*				97.69
#66		2	2.76 *0.49*	17.45 *0.03*	1.22 *0.07*	47.05 *1.07*	28.00 *1.48*	0.43 *0.03*	0.62 *0.02*	0.42 *0.10*	0.32 *0.08*	0.12 *0.01*				98.38
#45	Cpx	4	50.99 *0.49*	0.58 *0.12*	2.01 *0.48*		17.38 *0.66*	0.65 *0.09*	11.25 *0.44*	16.30 *0.49*	0.72 *0.13*	0.12 *0.08*				100.00
#65		3	50.98 *1.00*	0.56 *0.01*	1.75 *0.65*		16.85 *0.51*	0.61 *0.05*	11.39 *0.55*	17.13 *1.13*	0.59 *0.16*	0.12 *0.13*				99.99
#66		7	51.06 *0.92*	0.63 *0.08*	1.96 *0.76*		16.02 *1.01*	0.56 *0.05*	9.46 *0.77*	18.73 *0.96*	1.13 *0.42*	0.14 *0.08*				99.69

Table 2. continued

Run	Phase	n^a	SiO_2	TiO_2	Al_2O_3	Fe_2O_3	FeO	MnO	MgO	CaO	Na_2O	K_2O	P_2O_5	Cl	ZrO_2	Total
#45	Pl	(3)	69.19	0.45	16.65		2.90	b.d.	0.38	3.74	6.04	0.78				100.14
			1.80	*0.06*	*1.25*		*0.17*		*0.21*	*0.42*	*0.37*	*0.13*				
#65		3	64.80	0.36	19.03		3.04	b.d.	0.33	4.19	6.62	1.28				99.64
			0.73	*0.02*	*0.37*		*0.42*		*0.13*	*0.46*	*0.17*	*0.13*				
#66		7	64.84	0.25	19.59		2.41	b.d.	0.14	2.83	8.56	1.30				99.92
			0.94	*0.22*	*1.09*		*0.80*		*0.05*	*0.58*	*0.79*	*0.33*				
#45	Melt	(1)	76.14	1.35	11.08		3.20	0.00	0.92	2.71	3.94	0.55	0.06	0.05	b.d.	100.00
#65		2	71.54	0.63	12.40		4.82	0.13	0.44	1.86	4.19	2.80	0.09	0.90	0.22	100.00
			0.95	*0.04*	*0.18*		*0.21*	*0.02*	*0.22*	*0.37*	*0.39*	*0.02*	*0.01*	*0.01*	*0.01*	
#66		3	70.87	0.55	11.25		6.17	0.08	0.40	1.51	4.75	3.37	0.10	0.74	0.21	100.00
			0.42	*0.08*	*0.88*		*0.98*	*0.02*	*0.21*	*0.38*	*0.64*	*0.15*	*0.03*	*0.14*	*0.08*	
#81	Mag	2	0.19	2.09	1.27	29.22	61.53	0.70	1.40	0.28	b.d.	b.d.				96.67
			0.01	*0.00*	*0.01*	*0.12*	*0.17*	*0.02*	*0.00*	*0.00*						
#105		3	1.81	1.03	1.63	28.76	60.89	0.85	2.44	0.42	b.d.	0.06				97.89
			0.56	*0.01*	*0.1*	*0.44*	*1.03*	*0.09*	*0.19*	*0.3*		*0.02*				
#101		6	0.94	5.36	1.53	32.93	53.54	0.59	1.67	0.35	b.d.	0.02				96.95
			0.64	*0.08*	*0.04*	*0.5*	*1.52*	*0.05*	*0.16*	*0.18*		*0.02*				
#110		3	0.37	3.28	1.83	29.62	57.6	0.64	1.76	0.18	b.d.	b.d.				95.28
			0.12	*0.3*	*0.08*	*0.67*	*1*	*0.04*	*0.1*	*0.08*						
#81	Ilm	2	0.16	18.61	0.35	14.85	60.61	0.25	0.87	0.22	b.d.	b.d.				95.93
			0.01	*0.21*	*0.02*	*0.27*	*0.06*	*0.05*	*0.04*	*0.09*						
#105		5	0.19	15.67	0.51	11.77	67.67	0.26	1.13	0.16	b.d.	b.d.				97.36
			0.09	*0.53*	*0.04*	*0.42*	*0.89*	*0.04*	*0.05*	*0.02*						
#101		4	0.55	26.53	0.39	21.3	46.05	0.33	1.26	0.41	b.d.	0.04				96.86
			0.35	*0.31*	*0.07*	*0.41*	*0.66*	*0.03*	*0.07*	*0.17*		*0*				
#110		2	0.85	21.94	0.45	17.42	53.97	0.32	1.76	0.18	b.d.	b.d.				95.28
			1.01	*0.67*	*0.01*	*0.2*	*0.89*	*0.01*	*0.1*	*0.08*						
#81	Cpx	3	52.30	0.44	2.61		8.34	0.50	13.79	21.96	0.60	0.06				100.59
			0.15	*0.06*	*0.28*		*0.24*	*0.06*	*0.35*	*0.17*	*0.02*	*0.00*				
#105		3	51.15	0.71	3.4		8.95	0.44	12.52	21.96	0.62	0.06				99.80
			1	*0.1*	*0.29*		*0.17*	*0.06*	*0.24*	*0.44*	*0.08*	*0.02*				
#101		4	50.19	0.75	3.03		11.45	0.52	12.56	19.55	0.76	0.08				98.90
			0.87	*0.09*	*0.79*		*1.01*	*0.07*	*0.72*	*0.45*	*0.18*	*0.02*				
#110		9	50.36	0.64	2.96		8.77	0.46	13.32	22.15	0.61	0.04				99.32
			1.35	*0.13*	*0.74*		*1.26*	*0.06*	*0.64*	*0.75*	*0.16*	*0.01*				
#81	Pl	3	59.58	0.07	24.79		1.20	b.d.	b.d.	7.09	6.86	0.23				99.84
			0.96	*0.02*	*0.76*		*0.40*			*0.49*	*0.45*	*0.05*				
#105		5	60.34	0.11	24.51		1.06	b.d.	0.12	7.27	6.48	0.26				100.16
			0.87	*0.03*	*0.56*		*0.25*		*0.04*	*0.52*	*0.44*	*0.07*				
#101		8	60.86	0.21	24.05		1.42	b.d.	0.24	6.36	7.38	0.27				100.79
			1.17	*0.15*	*0.89*		*0.4*		*0.27*	*0.7*	*0.28*	*0.09*				
#110		10	58.18	0.04	27.6		0.76	b.d.	0.03	8.1	6.83	0.14				101.60
			1.21	*0.03*	*0.58*		*0.32*		*0.02*	*0.81*	*0.51*	*0.02*				
#81	Melt	12	74.25	0.31	14.59		1.41	0.08	0.23	1.85	5.26	1.80	b.d.	0.22	b.d.	100.00
			0.57	*0.05*	*0.18*		*0.18*	*0.01*	*0.04*	*0.15*	*0.43*	*0.08*		*0*		
#105		5	73.42	0.21	14.95		1.70	0.10	0.37	2.27	4.53	1.70	0.18	0.57	b.d.	100.00
			0.27	*0.04*	*0.29*		*0.28*	*0.03*	*0.05*	*0.2*	*0.42*	*0.04*	*0.15*	*0.1*		
#101		20	74.74	0.32	13.41		1.88	0.08	0.31	1.67	4.85	1.93	0.13	0.68	b.d.	100.00
			0.41	*0.04*	*0.27*		*0.21*	*0.02*	*0.06*	*0.16*	*0.24*	*0.11*	*0.13*	*0*		
#110		14	74.62	0.31	14.63		1.47	0.09	0.37	2.11	4.42	1.58	0.03	0.37	b.d.	100.00
			0.41	*0.05*	*0.27*		*0.25*	*0.01*	*0.05*	*0.09*	*0.3*	*0.08*	*0.03*	*0*		

Table 2. continued

Run	Phase	n^a	SiO_2	TiO_2	Al_2O_3	Fe_2O_3	FeO	MnO	MgO	CaO	Na_2O	K_2O	P_2O_5	Cl	ZrO_2	Total
#107	Mag	2	0.80	1.87	1.33	29.15	62.53	0.79	2.04	0.15	0.07	0.04				98.77
			0.65	*0.14*	*0.12*	*0.38*	*1.57*	*0.01*	*0.13*	*0.04*	*0.10*	*0.02*				
#103		4	0.72	6.58	1.36	34.19	51.20	0.60	1.25	0.25	b.d.	0.05				96.21
			0.32	*0.18*	*0.10*	*0.50*	*1.01*	*0.07*	*0.13*	*0.14*		*0.01*				
#111		2	0.73	4.33	1.43	32.22	57.04	0.62	1.53	0.27	0.04	0.02				98.26
			0.49	*0.05*	*0.15*	*0.39*	*0.90*	*0.06*	*0.07*	*0.15*	*0.06*	*0.03*				
#107	Ilm	3	0.37	20.06	0.33	15.35	58.40	0.35	1.38	0.25	b.d.	b.d.				96.49
			0.56	*1.65*	*0.02*	*0.97*	*3.05*	*0.02*	*0.15*	*0.24*						
#103		4	0.19	36.27	0.23	28.37	27.82	0.64	2.03	0.17	b.d.	b.d.				95.73
			0.08	*1.82*	*0.05*	*1.30*	*2.79*	*0.13*	*0.11*	*0.05*						
#111		9	0.14	26.06	0.32	20.47	48.20	0.31	1.38	0.18	b.d.	0.02				97.09
			0.10	*0.64*	*0.03*	*0.48*	*1.19*	*0.06*	*0.06*	*0.06*		*0.01*				
#107	Cpx	5	53.08	0.49	2.50		11.87	0.68	12.27	18.29	0.73	0.08				99.92
			1.84	*0.12*	*1.55*		*1.60*	*0.14*	*1.46*	*2.28*	*0.45*	*0.09*				
#103		6	51.39	0.41	1.67		12.59	0.76	13.35	17.91	0.57	0.02				98.64
			0.59	*0.08*	*0.19*		*1.02*	*0.14*	*0.85*	*1.48*	*0.08*	*0.01*				
#111		10	51.92	0.58	2.32		11.42	0.68	13.35	18.63	0.67	0.09				99.66
			1.18	*0.21*	*0.56*		*1.03*	*0.06*	*0.73*	*0.86*	*0.16*	*0.10*				
#107	Pl	4	63.18	0.15	23.57		1.11	b.d.	0.28	5.30	7.88	0.47				101.67
			0.23	*0.14*	*1.26*		*1.05*		*0.13*	*0.33*	*0.62*	*0.12*				
#103		5	62.34	0.41	21.49		2.92	b.d.	0.42	4.90	7.60	0.57				100.64
			1.32	*0.07*	*0.90*		*1.51*		*0.27*	*0.46*	*0.34*	*0.11*				
#111		8	62.85	0.13	22.93		1.22	b.d.	0.13	5.31	7.69	0.43				100.55
			1.39	*0.07*	*1.12*		*0.59*		*0.05*	*0.51*	*0.54*	*0.16*				
#107	Melt	4	78.06	0.25	12.29		1.88	0.08	0.28	1.06	2.64	2.67	0.14	0.53	0.12	100.00
			0.32	*0.07*	*0.51*		*0.49*	*0.02*	*0.09*	*0.13*	*0.18*	*0.02*	*0.05*	*0*	*0.04*	
#103		6	77.29	0.27	11.86		1.81	0.06	0.20	1.06	3.87	2.78	0.07	0.57	0.16	100.00
			0.47	*0.03*	*0.41*		*0.21*	*0.01*	*0.03*	*0.15*	*0.36*	*0.15*	*0.05*	*0*	*0.02*	
#111		10	78.59	0.26	11.62		1.43	0.07	0.23	1.12	3.77	2.19	0.08	0.54	0.10	100.00
			0.78	*0.03*	*0.51*		*0.13*	*0.01*	*0.06*	*0.25*	*0.37*	*0.1*	*0.07*	*0*	*0.02*	

Notes: Fe concentrations are given as FeO^{tot} (total iron), except for magnetite and Ilmenite, where Fe is given as Fe2O3/FeO contents; totals for melts are normalized to 100 wt%; *b.d.* below detection limit of the electron microprobe; σ standard deviation; for mineral abbreviations and run conditions see Table 1

[a]number of analyses

Table 3. Crystal sizes

run	temp. [°C]	cycling amplitude	aH_2O exp	median area (µm²) of the *n* largest crystals			
				n	Pl	*n*	Cpx
#42	950	static	0.98			*1*	70
#62	950	20 K	1.00			*1*	345
relative enlargement							***4.9***
#57	950	20 K	1.00			*1*	1348
relative enlargement							***19***
#43	950	static	0.39	*10*	54	*10*	7.3
#63	950	20 K	0.22	*10*	60	*10*	18
relative enlargement					***1.1***		***2.5***
#58	950	20 K	0.26	*10*	89	*10*	36
relative enlargement					***1.7***		***5.0***
#45	950	static	0.02	*10*	1.7	*10*	2.9
#65	950	20 K	0.02	*10*	9.3	*10*	7.1
relative enlargement					***5.6***		***2.5***
#66	950	20 K	0.06	*10*	114	*10*	9.8
relative enlargement					***69***		***3.4***
#105	800	static	0.96	*10*	20	*10*	22
#101	800	20 K	0.86	*10*	62	*10*	23
relative enlargement					***3.1***		***1.0***
#110	800	50 K	1.00	*10*	281	*10*	146
relative enlargement					***14***		***6.5***
#107	800	static	0.62	*10*	6.7	*10*	14
#103	800	20 K	0.44	*10*	24	*10*	40
relative enlargement					***3.5***		***2.8***
#111	800	50 K	0.50	*10*	41	*10*	47
relative enlargement					***6.1***		***3.3***

n number of measured crystals

For mineral abbreviations and calculation of aH_2O see Table 1

Single measurements of the 10 largest crystals are present in the deposit material

511

512

Figure 1

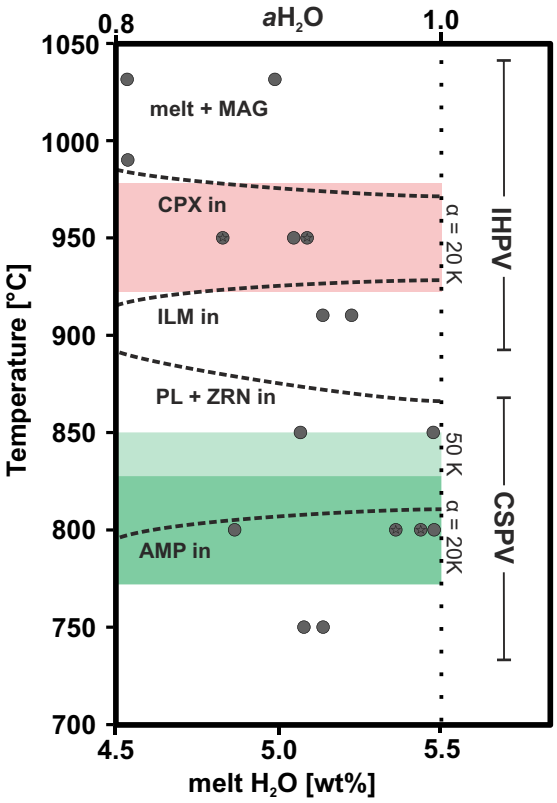
aH2O
0.8
1.0
1050
1000
950
900
850
800
750
700
melt + MAG
CPX in
ILM in
PL + ZRN in
AMP in
α = 20 K
50 K
α = 20K
IHPV
CSPV
Temperature [°C]
4.5
5.0
5.5
melt H2O [wt%]

Figure 2

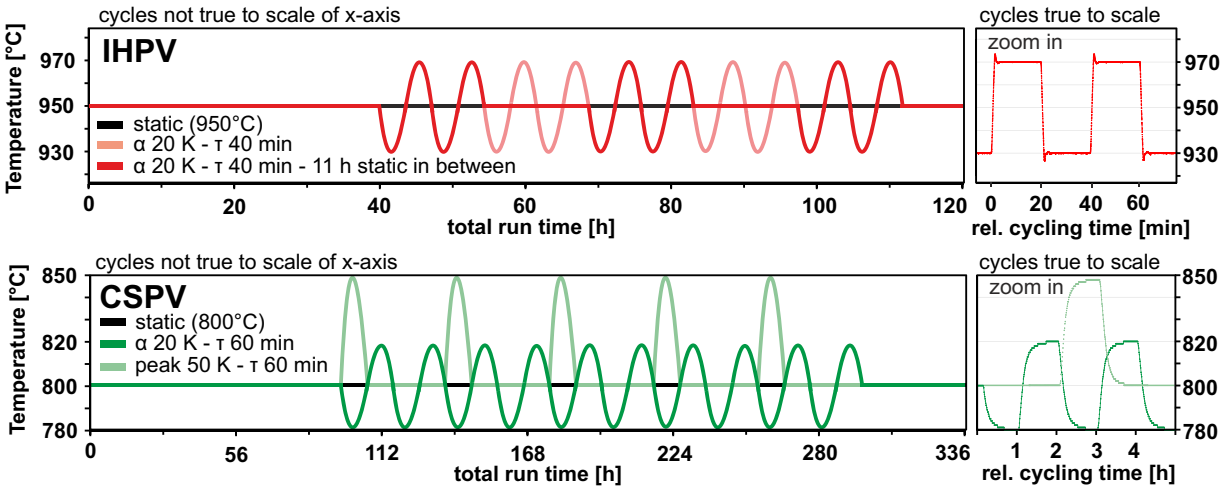
cycles not true to scale of x-axis
IHPV
static (950°C)
α 20 K - τ 40 min
α 20 K - τ 40 min - 11 h static in between
Temperature [°C]
970
950
930
0
20
40
60
80
100
120
total run time [h]
cycles true to scale
zoom in
0
20
40
60
rel. cycling time [min]
cycles not true to scale of x-axis
CSPV
static (800°C)
α 20 K - τ 60 min
peak 50 K - τ 60 min
Temperature [°C]
850
820
800
780
0
56
112
168
224
280
336
total run time [h]
cycles true to scale
zoom in
1
2
3
4
rel. cycling time [h]

Figure 3

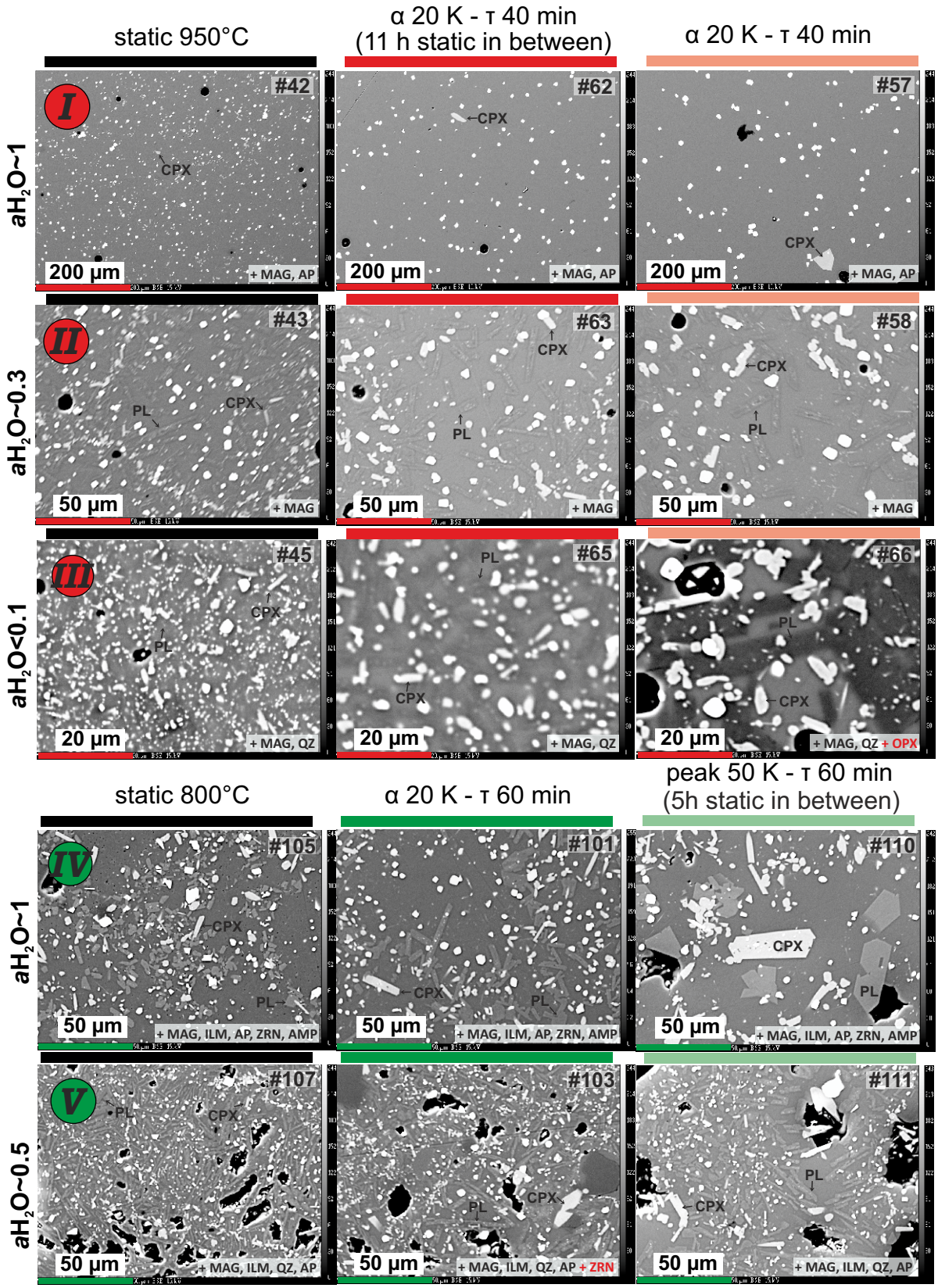
static 950°C
α 20 K - τ 40 min
(11 h static in between)
α 20 K - τ 40 min
aH2O~1
aH2O~0.3
aH2O<0.1
I
II
III
#42
#62
#57
#43
#63
#58
#45
#65
#66
CPX
PL
200 µm
50 µm
20 µm
+ MAG, AP
+ MAG
+ MAG, QZ
+ MAG, QZ + OPX
static 800°C
α 20 K - τ 60 min
peak 50 K - τ 60 min
(5h static in between)
aH2O~0.5
IV
V
#105
#101
#110
#107
#103
#111
+ MAG, ILM, AP, ZRN, AMP
+ MAG, ILM, QZ, AP
+ MAG, ILM, QZ, AP + ZRN

Figure 4

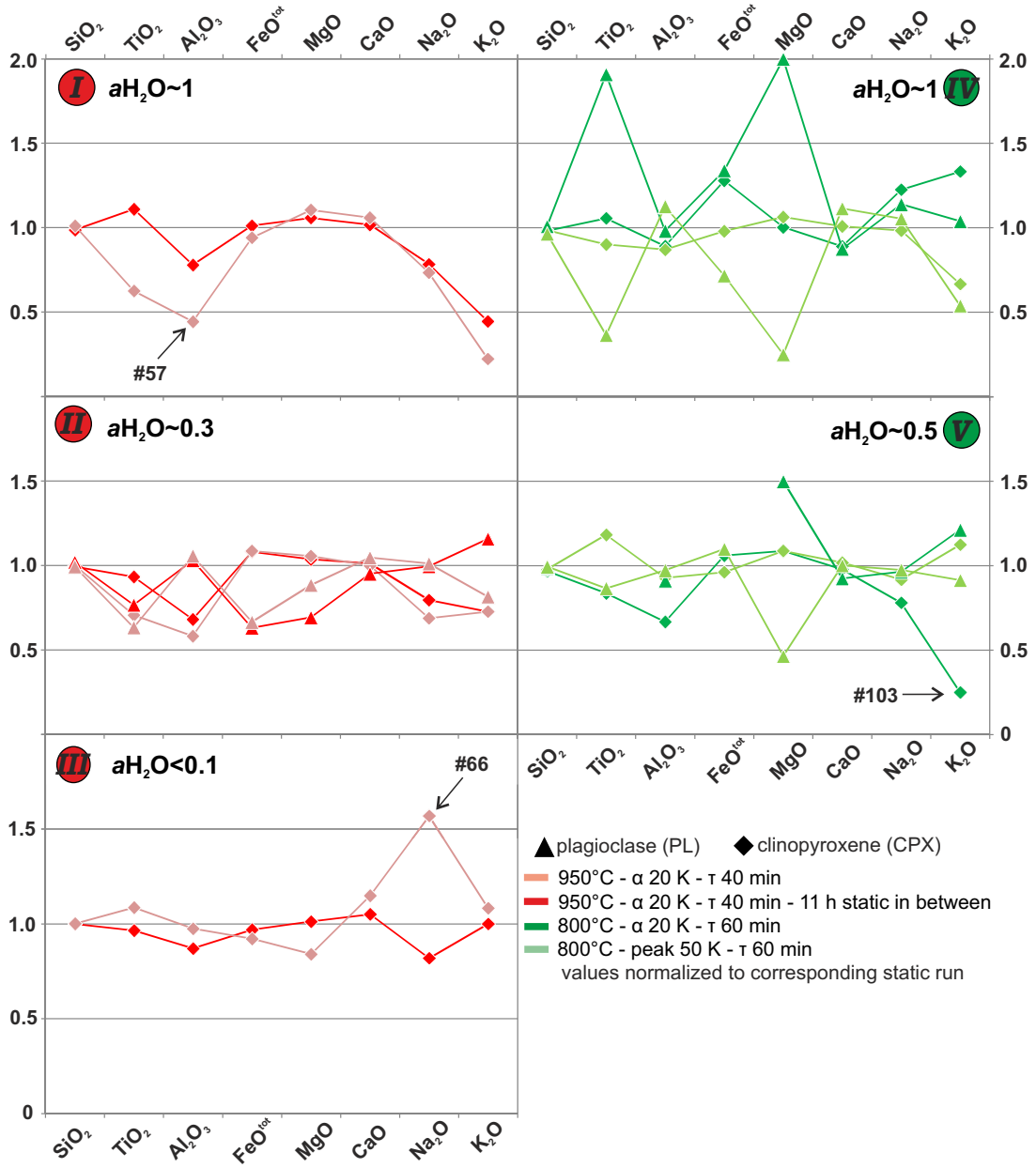
SiO2
TiO2
Al2O3
FeOtot
MgO
CaO
Na2O
K2O
I aH2O~1
II aH2O~0.3
III aH2O<0.1
IV aH2O~1
V aH2O~0.5
#57
#66
#103
2.0
1.5
1.0
0.5
0
plagioclase (PL)
clinopyroxene (CPX)
950°C - α 20 K - τ 40 min
950°C - α 20 K - τ 40 min - 11 h static in between
800°C - α 20 K - τ 60 min
800°C - peak 50 K - τ 60 min
values normalized to corresponding static run

Figure 5

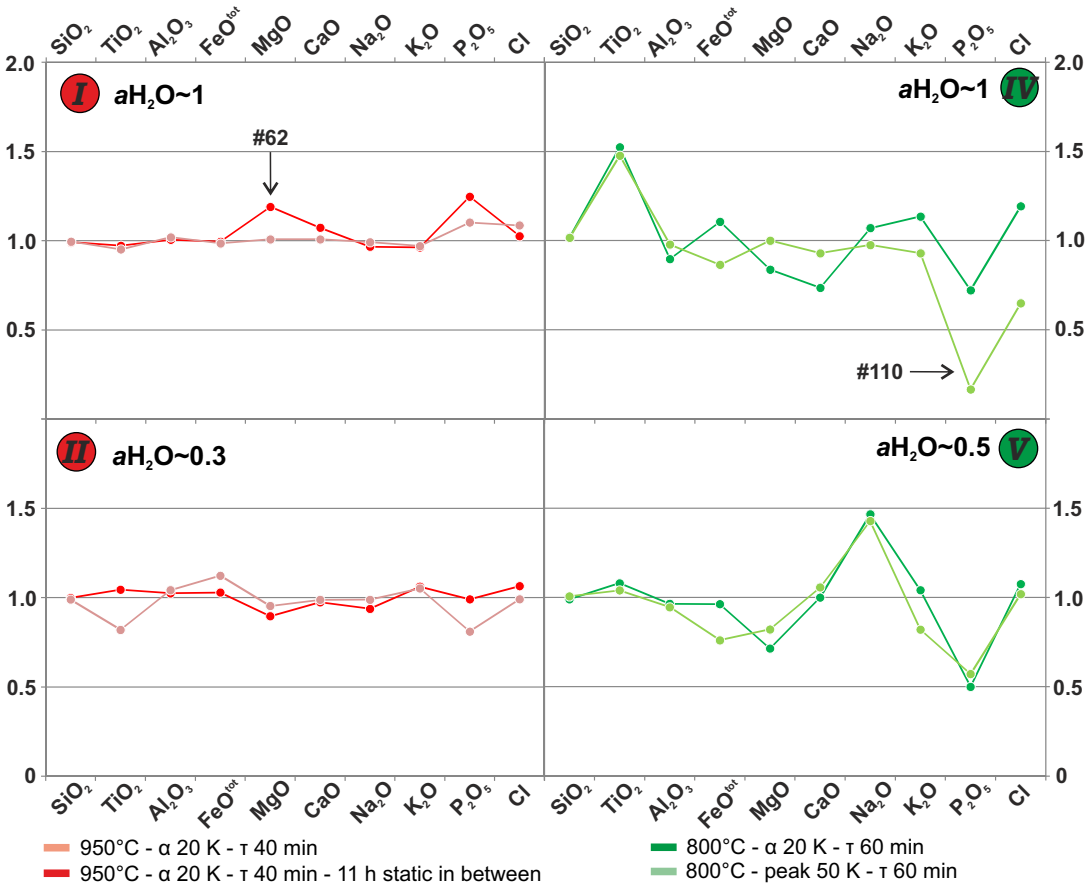
I aH2O~1
#62
IV aH2O~1
#110
II aH2O~0.3
V aH2O~0.5
SiO2 TiO2 Al2O3 FeOtot MgO CaO Na2O K2O P2O5 Cl
2.0
1.5
1.0
0.5
0
950°C - α 20 K - τ 40 min
950°C - α 20 K - τ 40 min - 11 h static in between
800°C - α 20 K - τ 60 min
800°C - peak 50 K - τ 60 min
values normalized to corresponding static run

Table 1. Experimental protocol

run	cycling type	P (MPa)	temp. (°C)	time (h)	TC (h)	H_2O[a] by-diff	$a\,H_2O$[b] exp	ΔQFM[c] exp	phase assemblages (proportions[d])
#42	static	200	950	120	-	5.1	0.98	+3.2	Melt(95.1), Mag(1.9), Cpx(1.2), Ap(1.8)
#62	TC	200	950±20	120	40	4.9	1.00	+3.2	Melt(96.6), Mag(2.2), Cpx(0.5), Ap(0.7)
#57	TC	200	950±20	120	72	5.1	1.00	+3.2	Melt(95.2), Mag(2.4), Cpx(0.9), Ap(1.5)
#43	static	200	950	120	-	2.6	0.39	+2.2	Melt(63.3), Mag(5.1), Cpx(6.0), Pl(25.6)
#63	TC	200	950±20	120	40	1.8	0.22	+1.9	Melt(66.6), Mag(3.1), Cpx(3.9), Pl(26.5)
#58	TC	200	950±20	120	72	2.0	0.26	+2.0	Melt(67.7), Mag(3.8), Cpx(4.4), Pl(24.1)
#45	static	200	950	120	-	0.5	0.02	-0.3	Melt(24.9), Mag(6.1), Cpx(20.9), Pl(44.1), Qz(4.0)
#65	TC	200	950±20	120	40	0.5	0.02	-0.1	Melt(24.3), Mag(5.7), Cpx(12.9), Pl(53.0), Qz(4.2)
#66	TC	200	950±20	120	72	0.8	0.06	+0.7	Melt(32.0), Mag(3.7), Cpx(15.2), Pl(47.5), Qz(1.6), Opx
#81	static	200	800	650	-	5.5	1.00	+0.6	Melt(72.5), Mag/Ilm(4.9), Cpx(8.2), Pl(14.4), Ap, Zrn
#105	static	200	800	336	-	4.8	0.86	+0.4	Melt(75.9), Mag/Ilm(3.8), Cpx(6.6), Pl(13.7), Ap, Zrn, Amp
#101	TC	200	800±20	336	192	5.5	1.00	+0.5	Melt(68.4), Mag/Ilm(5.7), Cpx(6.7), Pl(19.1), Ap, Zrn, Amp
#110	peak	200	800+50	336	192	5.4	1.00	+0.5	Melt(63.9), Mag/Ilm(3.0), Cpx(13.6), Pl(19.6), Ap, Zrn, Amp
#107	static	200	800	336	-	3.5	0.62	+0.1	Melt(46.7), Mag/Ilm(5.7), Cpx(10.8), Pl(30.9), Qz(6.0), Ap
#103	TC	200	800±20	336	192	2.8	0.43	-0.2	Melt(39.8), Mag/Ilm(6.1), Cpx(8.2), Pl(33.1), Qz(12.9), Ap, Zrn
#111	peak	200	800+50	336	192	3.1	0.50	-0.1	Melt(49.5), Mag/Ilm(6.6), Cpx(9.0), Pl(28.0), Qz(7.0), Ap

Mag magnetite, *Ilm* ilmenite, *Cpx* clinopyroxene, *Opx* orthopyroxene, *Pl* plagioclase, *Qz* quartz, *Ap* apatite, Amp amphibole, Zrn zircon

[a] determination via by-diference (following Devine et al. 1995) with electron microprobe (KFT-calibrated)

[b] water activity is calculated from the measured composition of the fluid phase

[c] ΔQFM indicates log $f\,O_2$ (experiment) - log $f\,O_2$ (QFM buffer) as estimated by Schwab and Küstner (1981)

[d] phase proportions in vol% (<0.5 vol % if not specified); determined via *ImageJ* (see text for details)

Table 2. Experimental results

Run	Phase	*n* [a]	SiO_2	TiO_2	Al_2O_3	Fe_2O_3	FeO	MnO	MgO	CaO	Na_2O	K_2O	P_2O_5	Cl	ZrO_2	Total
Starting		60	65.00	0.95	14.20		7.87	b.d.	1.46	4.58	4.45	1.18	b.d.	0.32	b.d.	100.00
composition			*0.51*	*0.05*	*0.21*		*0.36*		*0.14*	*0.20*	*0.26*	*0.05*		*0.02*		
#42	Mag	3	0.08	3.20	1.77	28.48	60.72	0.52	3.04	0.10	b.d.	b.d.				98.01
			0.07	*0.04*	*0.07*	*0.15*	*0.45*	*0.06*	*0.04*	*0.01*						
#62		7	0.13	3.08	1.64	27.97	61.96	0.50	3.51	0.10	b.d.	0.01				98.95
			0.04	*0.05*	*0.06*	*0.30*	*0.44*	*0.09*	*0.08*	*0.05*		*0.02*				
#57		2	0.06	4.28	1.77	29.84	58.22	0.44	2.76	0.07	b.d.	b.d.				97.44
			0.08	*0.02*	*0.01*	*0.01*	*0.64*	*0.00*	*0.09*	*0.10*						
#42	Cpx	5	51.84	0.64	2.89		7.74	0.33	14.01	21.51	0.60	0.09				99.64
			1.09	*0.11*	*0.65*		*0.65*	*0.05*	*0.64*	*0.86*	*0.10*	*0.05*				
#62		3	51.12	0.71	2.25		7.83	0.37	14.82	21.87	0.47	0.04				99.48
			0.24	*0.01*	*0.17*		*0.10*	*0.04*	*0.54*	*0.41*	*0.04*	*0.02*				
#57		2	52.38	0.40	1.28		7.28	0.33	15.48	22.78	0.44	0.02				100.37
			0.27	*0.01*	*0.06*		*0.04*	*0.01*	*0.19*	*0.33*	*0.01*	*0.01*				
#42	Melt	5	67.81	0.89	14.63		4.43	0.15	1.31	4.31	4.61	1.35	0.19	0.32	b.d.	100.00
			0.30	*0.05*	*0.12*		*0.23*	*0.02*	*0.07*	*0.08*	*0.19*	*0.06*	*0.01*	*0.00*		
#62		5	67.26	0.86	14.72		4.41	0.12	1.56	4.62	4.46	1.30	0.23	0.33	0.11	100.00
			0.27	*0.08*	*0.33*		*0.21*	*0.01*	*0.09*	*0.07*	*0.19*	*0.12*	*0.01*	*0.00*	*0.02*	
#57		4	67.52	0.85	14.92		4.37	0.13	1.32	4.34	4.58	1.31	0.21	0.35	0.11	100.00
			0.21	*0.05*	*0.38*		*0.15*	*0.03*	*0.04*	*0.04*	*0.22*	*0.03*	*0.03*	*0.00*	*0.02*	
#43	Mag	4	0.36	7.11	1.91	33.29	51.49	0.55	2.24	0.21	b.d.	0.01				97.18
			0.18	*0.24*	*0.06*	*0.58*	*1.20*	*0.03*	*0.11*	*0.10*		*0.02*				
#63		5	0.52	7.48	1.91	34.30	51.23	0.58	2.11	0.18	0.03	0.02				98.36
			0.26	*0.07*	*0.06*	*0.26*	*0.28*	*0.04*	*0.09*	*0.06*	*0.06*	*0.02*				
#58		3	0.58	8.75	1.93	35.53	47.84	0.51	2.00	0.28	b.d.	0.01				97.44
			0.60	*0.05*	*0.02*	*0.45*	*1.08*	*0.05*	*0.12*	*0.25*		*0.02*				
#43	Cpx	2	51.77	0.75	3.64		9.68	0.51	13.11	19.62	0.93	0.11				100.12
			0.14	*0.14*	*0.71*		*0.38*	*0.08*	*0.71*	*0.37*	*0.13*	*0.08*				
#63		7	51.42	0.70	2.48		10.47	0.54	13.59	19.85	0.74	0.08				99.86
			0.92	*0.07*	*0.52*		*0.67*	*0.10*	*0.35*	*0.37*	*0.19*	*0.05*				
#58		3	51.85	0.53	2.12		10.52	0.54	13.85	19.62	0.64	0.08				99.76
			0.82	*0.08*	*0.32*		*0.66*	*0.11*	*0.56*	*1.28*	*0.07*	*0.07*				
#43	Pl	5	60.11	0.30	21.95		3.23	b.d.	0.72	6.73	6.73	0.38				100.15
			0.77	*0.08*	*0.70*		*0.98*		*0.33*	*0.30*	*0.13*	*0.03*				
#63		5	61.37	0.23	22.63		2.04	b.d.	0.36	6.40	6.70	0.44				100.18
			1.09	*0.03*	*0.65*		*0.37*		*0.18*	*0.54*	*0.37*	*0.10*				
#58		3	59.74	0.19	23.21		2.15	b.d.	0.46	7.05	6.81	0.31				99.92
			0.26	*0.07*	*1.19*		*0.76*		*0.39*	*0.16*	*0.37*	*0.06*				
#43	Melt	3	72.64	0.67	13.04		3.25	0.10	0.58	2.10	5.15	1.73	0.12	0.44	0.17	100.00
			0.59	*0.05*	*0.52*		*0.12*	*0.00*	*0.08*	*0.30*	*0.04*	*0.13*	*0.02*	*0.02*	*0.01*	
#63		3	72.51	0.70	13.37		3.34	0.09	0.52	2.05	4.83	1.83	0.12	0.47	0.15	100.00
			0.47	*0.02*	*0.09*		*0.22*	*0.01*	*0.06*	*0.01*	*0.18*	*0.07*	*0.00*	*0.00*	*0.01*	
#58		3	71.89	0.55	13.59		3.65	0.11	0.55	2.07	5.10	1.82	0.10	0.44	0.13	100.00

			0.92	*0.01*	*0.47*		*0.21*	*0.01*	*0.08*	*0.25*	*0.44*	*0.17*	*0.01*	*0.02*	*0.02*	
#45	Mag	3	0.74	12.03	1.58	40.19	41.39	0.42	1.25	0.25	b.d.	b.d.				97.84
			0.48	*0.40*	*0.11*	*0.61*	*1.57*	*0.05*	*0.02*	*0.12*						
#65		3	1.84	12.62	1.86	40.22	38.70	0.40	0.96	0.59	0.43	0.06				97.69
			1.06	*0.78*	*0.43*	*0.96*	*1.65*	*0.05*	*0.50*	*0.52*	*0.40*	*0.03*				
#66		2	2.76	17.45	1.22	47.05	28.00	0.43	0.62	0.42	0.32	0.12				98.38
			0.49	*0.03*	*0.07*	*1.07*	*1.48*	*0.03*	*0.02*	*0.10*	*0.08*	*0.01*				
#45	Cpx	4	50.99	0.58	2.01		17.38	0.65	11.25	16.30	0.72	0.12				100.00
			0.49	*0.12*	*0.48*		*0.66*	*0.09*	*0.44*	*0.49*	*0.13*	*0.08*				
#65		3	50.98	0.56	1.75		16.85	0.61	11.39	17.13	0.59	0.12				99.99
			1.00	*0.01*	*0.65*		*0.51*	*0.05*	*0.55*	*1.13*	*0.16*	*0.13*				
#66		7	51.06	0.63	1.96		16.02	0.56	9.46	18.73	1.13	0.14				99.69
			0.92	*0.08*	*0.76*		*1.01*	*0.05*	*0.77*	*0.96*	*0.42*	*0.08*				
#45	Pl	(3)	69.19	0.45	16.65		2.90	b.d.	0.38	3.74	6.04	0.78				100.14
			1.80	*0.06*	*1.25*		*0.17*		*0.21*	*0.42*	*0.37*	*0.13*				
#65		3	64.80	0.36	19.03		3.04	b.d.	0.33	4.19	6.62	1.28				99.64
			0.73	*0.02*	*0.37*		*0.42*		*0.13*	*0.46*	*0.17*	*0.13*				
#66		7	64.84	0.25	19.59		2.41	b.d.	0.14	2.83	8.56	1.30				99.92
			0.94	*0.22*	*1.09*		*0.80*		*0.05*	*0.58*	*0.79*	*0.33*				
#45	Melt	(1)	76.14	1.35	11.08		3.20	0.00	0.92	2.71	3.94	0.55	0.06	0.05	b.d.	100.00
#65		2	71.54	0.63	12.40		4.82	0.13	0.44	1.86	4.19	2.80	0.09	0.90	0.22	100.00
			0.95	*0.04*	*0.18*		*0.21*	*0.02*	*0.22*	*0.37*	*0.39*	*0.02*	*0.01*	*0.01*	*0.01*	
#66		3	70.87	0.55	11.25		6.17	0.08	0.40	1.51	4.75	3.37	0.10	0.74	0.21	100.00
			0.42	*0.08*	*0.88*		*0.98*	*0.02*	*0.21*	*0.38*	*0.64*	*0.15*	*0.03*	*0.14*	*0.08*	
#81	Mag	2	0.19	2.09	1.27	29.22	61.53	0.70	1.40	0.28	b.d.	b.d.				96.67
			0.01	*0.00*	*0.01*	*0.12*	*0.17*	*0.02*	*0.00*	*0.00*						
#105		3	1.81	1.03	1.63	28.76	60.89	0.85	2.44	0.42	b.d.	0.06				97.89
			0.56	*0.01*	*0.1*	*0.44*	*1.03*	*0.09*	*0.19*	*0.3*		*0.02*				
#101		6	0.94	5.36	1.53	32.93	53.54	0.59	1.67	0.35	b.d.	0.02				96.95
			0.64	*0.08*	*0.04*	*0.5*	*1.52*	*0.05*	*0.16*	*0.18*		*0.02*				
#110		3	0.37	3.28	1.83	29.62	57.6	0.64	1.76	0.18	b.d.	b.d.				95.28
			0.12	*0.3*	*0.08*	*0.67*	*1*	*0.04*	*0.1*	*0.08*						
#81	Ilm	2	0.16	18.61	0.35	14.85	60.61	0.25	0.87	0.22	b.d.	b.d.				95.93
			0.01	*0.21*	*0.02*	*0.27*	*0.06*	*0.05*	*0.04*	*0.09*						
#105		5	0.19	15.67	0.51	11.77	67.67	0.26	1.13	0.16	b.d.	b.d.				97.36
			0.09	*0.53*	*0.04*	*0.42*	*0.89*	*0.04*	*0.05*	*0.02*						
#101		4	0.55	26.53	0.39	21.3	46.05	0.33	1.26	0.41	b.d.	0.04				96.86
			0.35	*0.31*	*0.07*	*0.41*	*0.66*	*0.03*	*0.07*	*0.17*		*0*				
#110		2	0.85	21.94	0.45	17.42	53.97	0.32	1.76	0.18	b.d.	b.d.				95.28
			1.01	*0.67*	*0.01*	*0.2*	*0.89*	*0.01*	*0.1*	*0.08*						
#81	Cpx	3	52.30	0.44	2.61		8.34	0.50	13.79	21.96	0.60	0.06				100.59
			0.15	*0.06*	*0.28*		*0.24*	*0.06*	*0.35*	*0.17*	*0.02*	*0.00*				
#105		3	51.15	0.71	3.4		8.95	0.44	12.52	21.96	0.62	0.06				99.80
			1	*0.1*	*0.29*		*0.17*	*0.06*	*0.24*	*0.44*	*0.08*	*0.02*				
#101		4	50.19	0.75	3.03		11.45	0.52	12.56	19.55	0.76	0.08				98.90

		0.87	*0.09*	*0.79*		*1.01*	*0.07*	*0.72*	*0.45*	*0.18*	*0.02*				
#110	9	50.36	0.64	2.96		8.77	0.46	13.32	22.15	0.61	0.04				99.32
		1.35	*0.13*	*0.74*		*1.26*	*0.06*	*0.64*	*0.75*	*0.16*	*0.01*				
#81 Pl	3	59.58	0.07	24.79		1.20	b.d.	b.d.	7.09	6.86	0.23				99.84
		0.96	*0.02*	*0.76*		*0.40*			*0.49*	*0.45*	*0.05*				
#105	5	60.34	0.11	24.51		1.06	b.d.	0.12	7.27	6.48	0.26				100.16
		0.87	*0.03*	*0.56*		*0.25*		*0.04*	*0.52*	*0.44*	*0.07*				
#101	8	60.86	0.21	24.05		1.42	b.d.	0.24	6.36	7.38	0.27				100.79
		1.17	*0.15*	*0.89*		*0.4*		*0.27*	*0.7*	*0.28*	*0.09*				
#110	10	58.18	0.04	27.6		0.76	b.d.	0.03	8.1	6.83	0.14				101.60
		1.21	*0.03*	*0.58*		*0.32*		*0.02*	*0.81*	*0.51*	*0.02*				
#81 Melt	12	74.25	0.31	14.59		1.41	0.08	0.23	1.85	5.26	1.80	b.d.	0.22	b.d.	100.00
		0.57	*0.05*	*0.18*		*0.18*	*0.01*	*0.04*	*0.15*	*0.43*	*0.08*		*0.01*		
#105	5	73.42	0.21	14.95		1.70	0.10	0.37	2.27	4.53	1.70	0.18	0.57	b.d.	100.00
		0.27	*0.04*	*0.29*		*0.28*	*0.03*	*0.05*	*0.2*	*0.42*	*0.04*	*0.15*	*0.05*		
#101	20	74.74	0.32	13.41		1.88	0.08	0.31	1.67	4.85	1.93	0.13	0.68	b.d.	100.00
		0.41	*0.04*	*0.27*		*0.21*	*0.02*	*0.06*	*0.16*	*0.24*	*0.11*	*0.13*	*0.01*		
#110	14	74.62	0.31	14.63		1.47	0.09	0.37	2.11	4.42	1.58	0.03	0.37	b.d.	100.00
		0.41	*0.05*	*0.27*		*0.25*	*0.01*	*0.05*	*0.09*	*0.3*	*0.08*	*0.03*	*0.01*		
#107 Mag	2	0.80	1.87	1.33	29.15	62.53	0.79	2.04	0.15	0.07	0.04				98.77
		0.65	*0.14*	*0.12*	*0.38*	*1.57*	*0.01*	*0.13*	*0.04*	*0.10*	*0.02*				
#103	4	0.72	6.58	1.36	34.19	51.20	0.60	1.25	0.25	b.d.	0.05				96.21
		0.32	*0.18*	*0.10*	*0.50*	*1.01*	*0.07*	*0.13*	*0.14*		*0.01*				
#111	2	0.73	4.33	1.43	32.22	57.04	0.62	1.53	0.27	0.04	0.02				98.26
		0.49	*0.05*	*0.15*	*0.39*	*0.90*	*0.06*	*0.07*	*0.15*	*0.06*	*0.03*				
#107 Ilm	3	0.37	20.06	0.33	15.35	58.40	0.35	1.38	0.25	b.d.	b.d.				96.49
		0.56	*1.65*	*0.02*	*0.97*	*3.05*	*0.02*	*0.15*	*0.24*						
#103	4	0.19	36.27	0.23	28.37	27.82	0.64	2.03	0.17	b.d.	b.d.				95.73
		0.08	*1.82*	*0.05*	*1.30*	*2.79*	*0.13*	*0.11*	*0.05*						
#111	9	0.14	26.06	0.32	20.47	48.20	0.31	1.38	0.18	b.d.	0.02				97.09
		0.10	*0.64*	*0.03*	*0.48*	*1.19*	*0.06*	*0.06*	*0.06*		*0.01*				
#107 Cpx	5	53.08	0.49	2.50		11.87	0.68	12.27	18.29	0.73	0.08				99.92
		1.84	*0.12*	*1.55*		*1.60*	*0.14*	*1.46*	*2.28*	*0.45*	*0.09*				
#103	6	51.39	0.41	1.67		12.59	0.76	13.35	17.91	0.57	0.02				98.64
		0.59	*0.08*	*0.19*		*1.02*	*0.14*	*0.85*	*1.48*	*0.08*	*0.01*				
#111	10	51.92	0.58	2.32		11.42	0.68	13.35	18.63	0.67	0.09				99.66
		1.18	*0.21*	*0.56*		*1.03*	*0.06*	*0.73*	*0.86*	*0.16*	*0.10*				
#107 Pl	4	63.18	0.15	23.57		1.11	b.d.	0.28	5.30	7.88	0.47				101.67
		0.23	*0.14*	*1.26*		*1.05*		*0.13*	*0.33*	*0.62*	*0.12*				
#103	5	62.34	0.41	21.49		2.92	b.d.	0.42	4.90	7.60	0.57				100.64
		1.32	*0.07*	*0.90*		*1.51*		*0.27*	*0.46*	*0.34*	*0.11*				
#111	8	62.85	0.13	22.93		1.22	b.d.	0.13	5.31	7.69	0.43				100.55
		1.39	*0.07*	*1.12*		*0.59*		*0.05*	*0.51*	*0.54*	*0.16*				
#107 Melt	4	78.06	0.25	12.29		1.88	0.08	0.28	1.06	2.64	2.67	0.14	0.53	0.12	100.00
		0.32	*0.07*	*0.51*		*0.49*	*0.02*	*0.09*	*0.13*	*0.18*	*0.02*	*0.05*	*0.02*	*0.04*	
#103	6	77.29	0.27	11.86		1.81	0.06	0.20	1.06	3.87	2.78	0.07	0.57	0.16	100.00

		0.47	*0.03*	*0.41*	*0.21*	*0.01*	*0.03*	*0.15*	*0.36*	*0.15*	*0.05*	*0.01*	*0.02*	
#111	10	78.59	0.26	11.62	1.43	0.07	0.23	1.12	3.77	2.19	0.08	0.54	0.10	100.00
		0.78	*0.03*	*0.51*	*0.13*	*0.01*	*0.06*	*0.25*	*0.37*	*0.1*	*0.07*	*0.03*	*0.02*	

Notes: Fe concentrations are given as FeO^{tot} (total iron), except for magnetite and Ilmenite, where Fe is given as Fe2O3/FeO contents; totals for melts are normalized to 100 wt%; *b.d.* below detection limit of the electron microprobe; σ standard deviation; for mineral abbreviations and run conditions see Table 1

[a]number of analyses

Table 3. Crystal sizes

run	temp. [°C]	cycling amplitude	*a* H_2O exp	median area (µm²) of the *n* largest crystals *n*	Pl	*n*	Cpx
#42	950	static	0.98			*1*	70
#62	950	20 K	1.00			*1*	345
relative enlargement							***4.9***
#57	950	20 K	1.00			*1*	1348
relative enlargement							***19***
#43	950	static	0.39	*10*	54	*10*	7.3
#63	950	20 K	0.22	*10*	60	*10*	18
relative enlargement					***1.1***		***2.5***
#58	950	20 K	0.26	*10*	89	*10*	36
relative enlargement					***1.7***		***5.0***
#45	950	static	0.02	*10*	1.7	*10*	2.9
#65	950	20 K	0.02	*10*	9.3	*10*	7.1
relative enlargement					***5.6***		***2.5***
#66	950	20 K	0.06	*10*	114	*10*	9.8
relative enlargement					***69***		***3.4***
#105	800	static	0.96	*10*	20	*10*	22
#101	800	20 K	0.86	*10*	62	*10*	23
relative enlargement					***3.1***		***1.0***
#110	800	50 K	1.00	*10*	281	*10*	146
relative enlargement					***14***		***6.5***
#107	800	static	0.62	*10*	6.7	*10*	14
#103	800	20 K	0.44	*10*	24	*10*	40
relative enlargement					***3.5***		***2.8***
#111	800	50 K	0.50	*10*	41	*10*	47
relative enlargement					***6.1***		***3.3***

n number of measured crystals

For mineral abbreviations and calculation of *a* H_2O see Table 1

Single measurements of the 10 largest crystals are present in the deposit material